energies

MDPI

Article

Energy Independence of a Small Office Community Powered by Photovoltaic-Wind Hybrid Systems in Widely Different Climates

Nicoletta Matera [1], Domenico Mazzeo [2], Cristina Baglivo [1,*] and Paolo Maria Congedo [1]

[1] Department of Engineering for Innovation, University of Salento, 73100 Lecce, Italy; materanicoletta@gmail.com (N.M.); paolo.congedo@unisalento.it (P.M.C.)
[2] Department of Energy, Politecnico di Milano, 20156 Milan, Italy; domenico.mazzeo@polimi.it
* Correspondence: cristina.baglivo@unisalento.it

Abstract: Hybrid renewable energy systems are an optimal solution for small energy communities' energy supply. One of the critical issues is the strong correlation of these systems with outdoor climatic conditions. The goal is to make local communities increasingly energy independent. To this end, an in-depth analysis of the behaviour of hybrid photovoltaic (PV)–wind systems powering small office communities in 48 locations around the world characterized by widely varying climates was conducted. System sizes, assumed to be stand-alone or grid-connected, were varied, for a total of 343 system power configurations. Highest satisfied load fraction (SLF) values are obtained with a significant predominance of PV over wind; the trend is more pronounced in dry and continental climates (zones B and D according to the Köppen climate classification). The utilization factor (UF) values of 1 are rarely reached and never in the wind-only or PV-only configurations. In all climates, the grid energy interaction factor (GEIF) values of zero are never reached but come very close. The benefit-cost ratio (BCR) of grid-connected systems is significantly higher than stand-alone systems.

Keywords: district; hybrid renewable systems; battery; electric vehicle charging; offices; benefit–cost ratio; photovoltaic-wind; Köppen climate classification; satisfied load fraction; utilization factor

Citation: Matera, N.; Mazzeo, D.; Baglivo, C.; Congedo, P.M. Energy Independence of a Small Office Community Powered by Photovoltaic-Wind Hybrid Systems in Widely Different Climates. *Energies* **2023**, *16*, 3974. https://doi.org/10.3390/en16103974

Academic Editor: Haixiao Liu

Received: 13 March 2023
Revised: 25 April 2023
Accepted: 5 May 2023
Published: 9 May 2023

1. Introduction

Extreme and sudden events are increasingly occurring in cities, which are hotspots for climate impacts. The analysis of cities involves many variables, making such analysis very complex [1,2]. Urban resilience refers to the ability of cities to cope with disasters and sudden events [3,4], protecting infrastructure, economic structures, and technical systems [5]. Cities cannot completely avoid unforeseen dangers, but they can become more resilient to them. Cities can be virtuous forces in managing change. In this case, the threat is not purely negative but can be a catalyst for change, innovation, and development [6].

Planners, policymakers, and researchers have begun to use the term resilience in discussions of urban regeneration, redevelopment, and planning. This makes it a crucial concept for urban design and planning [7]. The concept of resilience is closely related to sustainable development. Cities' sustainability and resilience can be assessed by considering a wide range of subsystems, including the economy, environment, population, resources, science, and technology [8]. Natural disasters and extreme weather conditions are unavoidable and can negatively affect socioeconomic activities, energy security, and quality of life. A resilient power grid is critical to reducing disaster impacts [9]. Security measures must ensure that the power system can withstand the most severe damage and operate without interruption or with minimal interruption. The study [10] showed that security can reduce total costs when catastrophic events occur. Threats to electrical system security can be short-term or long-term [11]. The short-term threat to an electrical system

can be caused by sudden disturbances that occur unexpectedly at a given time [12]. Environmental load, fuel depletion, or increased energy consumption can all contribute to the long-term threat to the energy system [13].

The depletion of fossil fuels and increasing worries about global warming have spurred the adoption of renewable energy sources [14], not only in urban settings but also in rural communities [15]. Buildings are expected to suffer from rising temperatures in the years to come, especially in hot and torrid climates [16].

Renewable energies offer a viable alternative to conventional energy [17–19]. An important issue to address is the intermittency and unpredictability of these systems due to their strong dependence on weather and climate conditions [20]. For example, stand-alone photovoltaic (PV) or wind systems meet load demand only as long as solar radiation or adequate wind speed is available [21]. As a result, when renewable energy systems are used, a backup energy source and/or storage system is generally needed to provide energy when renewable sources are not available [22]. Therefore, hybrid systems are developed to complement different alternative energy sources. In this direction, optimal sizing of hybrid systems ensures high quality and better reliability than a system powered by a single energy source. Hybrid systems are crucial for electrifying remote areas [23], particularly because reports from the World Bank and IEA [24,25] reveal that approximately 22 percent of the world's population does not have access to the national power grid. Economic studies have shown that these technologies are particularly advantageous for developing countries [26].

Building energy independence increases with hybrid systems consisting of photovoltaics and storage [27]. Khan et al. [28] addressed the problem of remote rural electrification with the goal of achieving continuous power supply to meet variable load demand under different weather conditions. They identified the optimal hybrid renewable energy system (HRES) configuration from an economical and high-reliability point of view. El-Sattar [29] analyzed hybrid systems based on the integration of biomass with PV, wind, and battery. They conducted optimizations in order to minimize the cost of energy by improving the energy supply, focusing on rural areas.

In the literature, reliability assessments place more emphasis on static conditions than dynamic responses to sudden disturbances. For autonomous renewable hybrid systems, an assessment of resilience after an unexpected interruption is essential.

In the work [30], the impact of storage capacity on the resilience of an independent hybrid renewable system during unexpected breakdowns was investigated. The study found that the system's resilience decreased in a nonlinear manner as the frequency and duration of failures increased.

This study investigates the resilience of PV–wind hybrid plants designed for a small office community. It is assumed that plants are to be located in several locations evenly distributed around the world. This goal is pursued through hourly and annual dynamic analyses of the hybrid system. Sustainability is assessed through technical and economic indicators.

2. Materials and Methods

This section outlines the main steps covered in this study, which can be summarized as follows:

- Selection of cities homogeneously distributed throughout the world across the Köppen climate classification (Section 2.1)
- Definition of a reference office district (Section 2.2)
- Characterization of the hybrid system (Section 2.3)
- Numerical modelling of the hybrid system in TRNSYS (Section 2.4)
- Technical and economic analysis (Section 2.5)
- Parametric analysis (Section 2.6).

2.1. Selection of Cities

Figure 1 presents the 48 selected localities characterized by different latitudes and altitudes. The locations are listed in accordance with their Köppen climate classification [31,32]. Kano is the sunniest location, with upper-middle wind speed. Tromsø is very low sunny. Milan, Moscow, and Oymyakon have low solar radiation and wind speed. Lihue, Nairobi, Mombasa, and Recife have high solar radiation and wind speed. Auckland and Wellington are the windiest. Recife is the warmest city and Oymyakon the coldest.

Köppen Group	Köppen sub-group	Locality	Country
A *Tropical Megathermal climates*	**Af** *Tropical rainforest climate*	Toamasina	Madagascar
		Singapore	Singapore
	Am *Tropical monsoon climate*	Recife (Pernambuco)	Brazil
		Miami (Florida)	USA
	As *Tropical dry or savanna climate*	Lihue (Hawaii)	USA
		Mombasa	Kenya
	Aw *Tropical wet or savanna climate*	Caracas	Venezuela
		Kano	Nigeria
B *Dry (desert and semi-arid) climates*	**BWh** *Desert climate*	Baghdad	Iraq
		Cairo	Egypt
	BSk *Semi-arid, cold climate*	Kabul	Afghanistan
		Baku	Azerbaijan
	BSh *Semi-arid, hot climate*	Odessa (Texas)	USA
		Maracaibo	Venezuela
C *Temperate Mesothermal climates*	**Cfa** *Humid subtropical climates, without dry season*	Buenos Aires	Argentine
		Milan	Italy
	Cfb *Oceanic climate, warm summer*	Berlin	Germany
		London	UK
		Vancouver (British Columbia)	Canada
		Melbourne (Victoria)	Australia
		Bogotá (Cundinamarca)	Colombia
		Wellington	New Zeland
	Cfc *Subpolar oceanic climates*	Reykjavík	Islands
		Auckland	New Zeland
	Csa *Mediterranean climates, hot summer*	Rome	Italy
		Adelaide	Australia
	Csb *Mediterranean climates, warm summer*	Porto	Portugal
		La Coruna	Spain
	Cwa *Humid subtropical climates, dry winter*	New Delhi	India
		Hong Kong	China
	Cwb *Highland climates*	Johannesburg	South Africa
		Nairobi	Kenya
D *Continental Microthermal climates*	**Dfa** *Hot summer continental climates, without dry season*	Bucharest	Romania
		Toronto (Ontario)	Canada
	Dfb *Warm summer continental climates, without dry season*	Moskva	Russia
		Ottawa (Ontario)	Canada
	Dfc *Subarctic or boreal climates*	Tromsø	Norway
		Anchorage (Alaska)	USA
	Dfd *Subarctic or boreal climates*	Oymyakon (Sakha Republic)	Russia
		Verhojansk (Sakha Republic)	Russia
	Dsa *Hot summer continental climates, dry summer*	Hakkâri	Turkey
		Cambridge (Nunavut)	Canada
	Dsb *Warm summer continental climates, dry summer*	Dras	India
		Flagstaff (Arizona)	USA
	Dwa *Hot summer continental climates, dry winter*	Beijing	Cina
		Seoul	South Korea
	Dwb *Warm summer continental climates, dry winter*	Pyongyang	North Korea
		Vladivostok	Russia

Figure 1. List of locations with their climates.

2.2. Definition of the Reference Office District

The hybrid system is investigated to serve a small district consisting of five identical office buildings. The choice of office use allows for standardized building occupancy profiles in all selected cities. The buildings are composed of two 100 m^2 floors with large windows. Each building consists of eight thermal zones, i.e., eight rooms with different orientations and occupant profiles. During all working days: six zones are occupied both in the morning and afternoon, while two zones are occupied only in the morning. The energy required by the district comes from lighting, office equipment, and electric vehicle charging stations. Hybrid systems do not meet the energy needs of heating, cooling, and domestic hot water systems as these systems do not run on electricity.

Each thermal zone has its weekly load profile; with occupants, each zone needs 75 W to power two computers and a printer. The LED lighting system requires 125 W. The lights turn on when users occupy rooms and solar radiation levels fall below a set value. As the assumed district is sited in locations with very different climates, the load varies according to solar radiation. A differential controller enables intelligent on/off management.

Each building in the district provides four electric vehicle charging stations, for a total of 20 charging stations throughout the district. Forty Nissan Leaf electric vehicles are provided, each vehicle needing a charging time of two hours to replenish its daily power consumption of 5.14 kWh, resulting from an average daily mileage of 26.8 km and a charging efficiency of 0.1714 kWh/km [33]. The charging stations used to charge these vehicles have a power rating of 2.3 kW. Therefore, 20 cars will be recharged from 9 a.m. to 11 a.m. and the other 20 from 11 a.m. to 1 p.m. Electric vehicle charging is the largest contributor to the districts' annual load [34].

2.3. The Hybrid System

This section will detail the primary characteristics of the photovoltaic, wind, and battery elements that comprise the hybrid system. It should be noted that both grid-connected (GC) and stand-alone (SA) hybrid systems are analyzed in this study.

The PV module used in this study is the Mitsubishi Electric PV-MLU250HC [35], which is composed of polycrystalline silicon cells and has a rated power of 250 W, an operating efficiency of 15.3%, a nominal operating temperature (NOCT) of 46 °C, and a surface area of 1.6236 m^2.

The wind microgenerator [36] installed on the rooftop of the building (14.5 m above the ground) has a rated power of 2500 W, and its starting, rated, and stopping speeds are 3 m/s, 10 m/s, and 18 m/s, respectively.

The battery considered is a lithium-ion battery of the SonnenBatterie type [37], with a capacity equal to 10 kWh and an efficiency of 0.98.

The efficiencies of the inverter FRONIUS IG PLUS V DC/AC [38], DC/DC converter, AC/DC rectifier, and regulator are 0.97, 0.94, 0.90, and 0.98, respectively.

The methodology permits consideration of the real storage capacity during its use, as well as the PV degradation with time. In particular, for each scenario, the dynamic power simulation of the system would be performed each year with the new PV efficiency (or power at the maximum power point) and the new storage capacity. So, for example, if the lifespan of the investment is 30 years, for each scenario, 30 energy simulations are required. Consequently, 30 yearly economic and environmental analyses are required. Usually, a linear trend to take into account these degradations is used.

For this research, the photovoltaic system's average efficiencies, specifically the maximum power point, and the storage battery's capacities were considered throughout the investment's entire lifespan [34].

Excess energy is stored in the storage system. Later, the excess is sent to the grid for GC and lost in SA systems.

When the hybrid system generates energy in excess, compared to that required by the district, it is sent to the battery. The excess is dissipated for the SA system and sent to the grid for the GC system.

When the hybrid system cannot meet the demands of the district, it is taken from the battery. For the SA system, energy can be supplemented with a diesel generator; for the GC system, it can be drawn from the grid.

An in-depth study of the costs of the different components of the hybrid system was carried out in a previous paper [34]. The annual system-specific purchase costs of the hybrid system components are expressed in €/kW and are calculated as a function of installed rated power. Empirical equations were derived by adjusting specific purchase costs for different power ratings. Different power ratings of the same type of system were considered for photovoltaic, battery, and inverter systems. Different types of micro-wind generators were considered since Tulipower is only available in the market for 2.5 kW.

A comprehensive study of national electricity systems was conducted to capture the average annual price of electricity for non-domestic use for all selected countries.

2.4. Numerical Modeling of the Hybrid System in TRNSYS

TRNSYS 17 [39] was used to model the hybrid system with all its components and evaluate its hourly and annual behaviour. Type 94a allows photovoltaic electrical performance to be determined with a five-parameter model [40]. Type 90 calculates wind turbine power output as a function of wind speed, using the Quinlan equations [41]. Type 47 allows the modelling of lithium-ion batteries and calculating the state of charge (SOC) as a function of time, known charge, and discharge rates. Type 48 is used for regulator and inverter simulations, Type 2 for differential lighting controllers, and Type 15 for tm2 climate data import. The procedure used to characterize the behaviour of the PV module, wind generator, and storage battery is extensively explained in the paper [42]. Figure 2 presents a synthetic scheme for the PV–wind hybrid system.

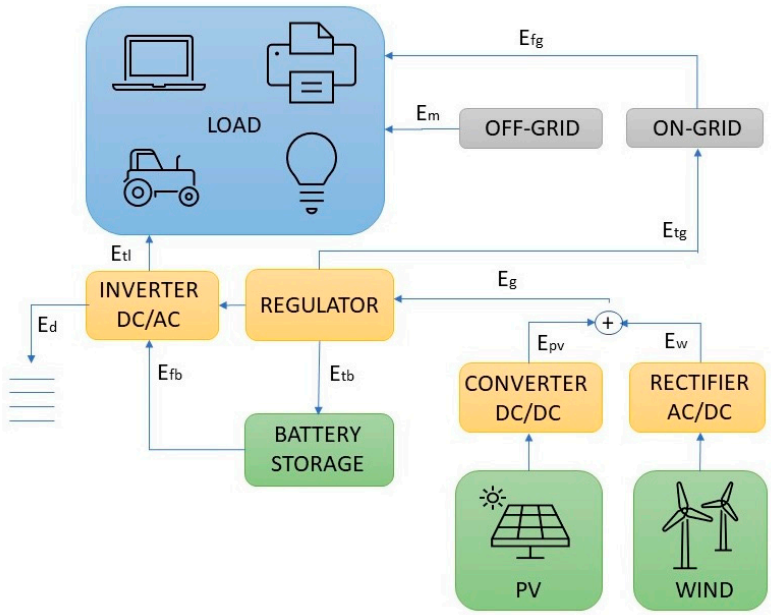

Figure 2. Scheme of the PV-wind hybrid system.

2.5. Technical and Economic Parametric Analysis

The parameters for the technical and economic analysis of the hybrid system are presented in this section.

Equation (1) reports the load-satisfied fraction (SLF), calculated as the ratio between the yearly produced energy sent to the load (E_{tl}) and the yearly energy required by the load (E_l). When SLF is equal to 1, the annual energy required by the load is fully supplied by the hybrid system.

$$SLF = \frac{E_{tl}}{E_l} \quad (1)$$

Equation (2) presents the utilization factor (UF), calculated as the ratio between the yearly produced energy sent to the load (E_{tl}) and the yearly energy produced by the generators (E_g). When UF is equal to 1, the annual energy generated is entirely used to meet the load.

$$UF = \frac{E_{tl}}{E_g} \tag{2}$$

Equation (3) reports the grid energy interaction factor (GEIF). This value indicates the interaction of the system with the grid; for example, when GEIF is equal to 0 there is no interaction with the grid, i.e., the load does not draw energy from the grid and does not supply energy to the grid when there is an excess of energy.

$$GEIF = (1 - SLF) + (1 - UF)\frac{E_g}{E_l} \tag{3}$$

For the economic aspect, the non-discount benefit-cost ratio (BCR) was calculated, which is a dimensionless index used to identify optimal system configurations.

$$BCR = \frac{B}{C} \tag{4}$$

The capital cost (C) is the sum of the initial cost and replacement cost of system components. This study considers economies of scale, which allow for the correlation of increasing system size with decreasing system unit cost. In this way, the purchase cost of a system component in €/kW varies with the installed power of the system.

As for benefit (B), this varies depending on whether the system is stand-alone or grid-connected. Specifically, for stand-alone hybrid systems, the economic value is related to the energy produced and sent to the load.

For grid-connected hybrid systems, the benefit is the combination of costs related to the electricity generated by the hybrid system and supplied to the load, as well as revenue earned from selling surplus solar and wind power to the grid through the Feed-in-Tariff (FiT). The economic assessment was carried out at the start of the investment, hence operational expenses, system maintenance costs, discount rate, and inflation rate were not taken into account.

We carried out an economic analysis of the hybrid system on a global scale, which involved conducting an economic assessment for each of the 48 different locations examined in this study. The aim was to determine the optimal power configuration for the hybrid system in each location and identify the most economically feasible location for either a stand-alone or a grid-connected hybrid system. To achieve this, we gathered all the relevant information on electricity purchasing tariffs and feed-in-tariffs for selling excess energy, as well as specific costs for purchasing system components, and evaluated economies of scale based on market trends on a country-by-country basis.

In summary, the analysis can be summarized as follows:

- Empirical equations were used to determine the annual specific costs, expressed in €/kW, for purchasing PV, wind, battery, and inverter systems, based on the installed nominal power. These equations were obtained by fitting specific purchase costs for various nominal powers obtained from the market. Reference [34] provides additional data and references related to this market analysis.
- To determine the yearly average electricity price for non-household use in the countries examined in this study, a comprehensive analysis of each nation's electrical systems was conducted. The data collection process, along with additional information and references, is thoroughly documented in [34].
- Likewise, a thorough research effort was undertaken to gather global data on Feed-in Tariff (FiT) electricity policies. These policies involve compensating renewable energy producers for the excess energy they sell to the national grid, based on the cost of

production. Additional details and references related to this data collection can be found in reference [34].

2.6. Parametric Analysis

Parametric analysis was developed for all selected cities. A total of seven configurations were chosen for each of the main components (PV, wind, battery) of the hybrid system. The total power of each component varied from 10 kW to 130 kW in 20 kW steps. The PV system consists of 40 panels of 250 W for a total of 10 kW. As mentioned above, they have varied their total power from 10 kW to 130 kW with a step of 20 kW. This results in 1, 3, 5, 7, 9, 11, and 13 strings in parallel. Similarly, the single wind turbine being 2.5 kW, the seven configurations involve 4, 12, 20, 28, 36, 44, and 52 wind turbines. The batteries are 10 kW each, so the seven configurations are 1, 3, 5, 7, 9, 11, and 13.

This results in a total of 343 system configurations for each location, consisting of 7 PV configurations, 7 wind configurations, and 7 battery configurations. In total, for all 48 selected locations, the configurations become 16,464.

Using TRNSYS, the hourly power values of each system component were computed. These values were then used to determine the annual energy contributions for both the stand-alone and grid-connected systems' energy balances.

For all localities, an energy optimization was conducted, by following the energy-constrained reliability methods [42].

In the case of stand-alone power plants (SA), the focus is on meeting the energy demands of the load while minimizing any excess energy production. The optimal location for a stand-alone power plant is determined by the highest UF value.

In the case of grid-connected power plants (GC), it is necessary to limit both the energy drawn from the grid and the excess energy produced. This can be achieved by minimizing the GEIF value. The optimal location for a grid-connected power plant is determined by the lowest GEIF value, which is an indicator of the site's suitability for this purpose.

3. Results

The outcome of the parametric analysis was presented in relation to three key indicators: the satisfied load fraction (SLF), utilization factor (UF), and grid energy interaction factor (GEIF). In addition, the benefit-cost ratio (BCR) is shown for all configurations.

Figures 3–7 show the parametric analysis results by plotting the PV energy fraction ($e_{pv,g}$) on the x-axes. It is a dimensionless power parameter calculated as the ratio between PV power and the sum of PV and wind power.

Within each graph, the total number of configurations represented is equal to 343 energy system configurations for the number of cities within that climate zone.

Figure 3 shows the SLF of 343 system power configurations. Each quadrant represents a Köppen–Geiger area.

The aim is to determine the configurations that achieve high SLF values, as this ensures that the hybrid system can provide maximum energy production to meet the load demand.

It can be seen that the highest SLF values are obtained with a significant prevalence of PV over wind power, the trend being more pronounced for climate zones B and D. Climate A and climate C achieve an SLF value of 1 from PV energy fraction of 0.2, while climates B and D from PV energy fraction of 0.5. For all climate zones, there is evidence of the impracticality of reaching very high SLF values with a low PV fraction while simultaneously reducing the oscillation by maintaining high average values. In conclusion:

- Group A is characterized by satisfied load fractions variable between 0.4 and 0.9 for $e_{pv,g} < 0.1$ and between 0.5 and 1 for $e_{pv,g} \approx 1$
- Group B variable between 0.3 and 0.9 for $e_{pv,g} < 0.1$ and between 0.9 and 1 for $e_{pv,g} \approx 1$
- Group C variable between 0.3 and 0.9 for $e_{pv,g} < 0.1$ and between 0.3 and 1 for $e_{pv,g} \approx 1$
- Group D variable between 0.2 and 0.9 for $e_{pv,g} < 0.1$ and between 0.3 and 1 for $e_{pv,g} \approx 1$.

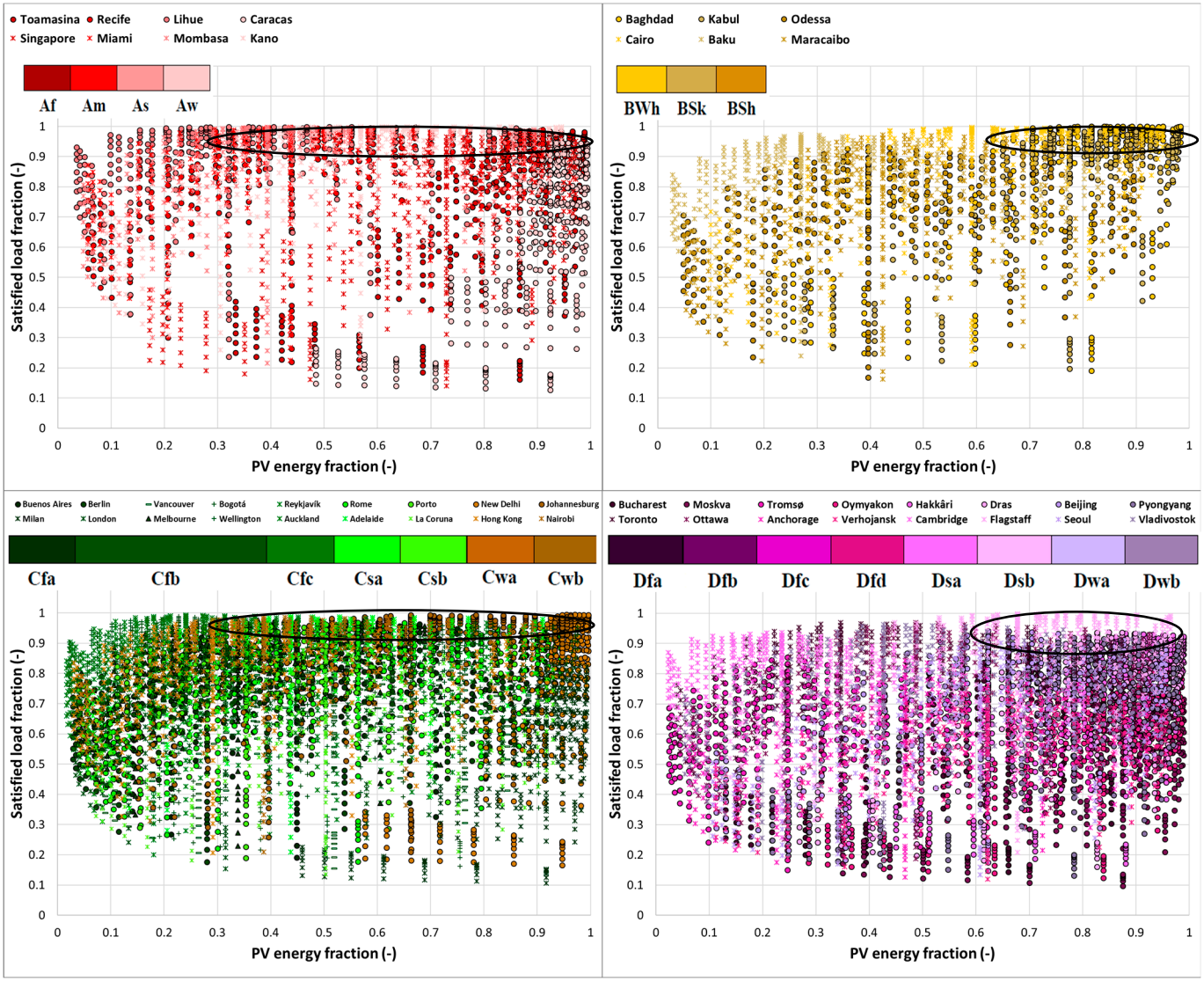

Figure 3. Satisfied load fraction of 343 system power configurations across Köppen-Geiger climates.

Figure 4 shows the UF of all system power configurations. When UF = 1, the yearly energy generated is entirely used to satisfy the load. The range of variation in these parameters grows with an increasing PV energy fraction. Quantitatively, Group B points are concentrated in lower utilization factors than the other groups, denoting high energy excess. For Groups A, C, and D, a strong concentration is evident for high values of PV energy fraction and tendentially lower values of utilization fraction.

Values of UF equal to 1 are rarely achieved and never by extreme values of PV energy fraction (and thus considering only wind or only PV contributions). In detail, in climate zone A, a UF value of 1 is reached for some configurations between 0.7 and 0.9 PV energy fractions. In climate B, the UF value of 1 is never reached. In climate C, the UF value of 1 is achieved with PV energy fraction values between 0.85 and 0.95. The UF value of 1 is achieved in climate D for PV energy fraction between 0.7 and 0.9. The UF value of 1 is achieved in climate D with PV energy fraction values between 0.7 and 0.9. UF values below 0.1 are not achieved, for any climate.

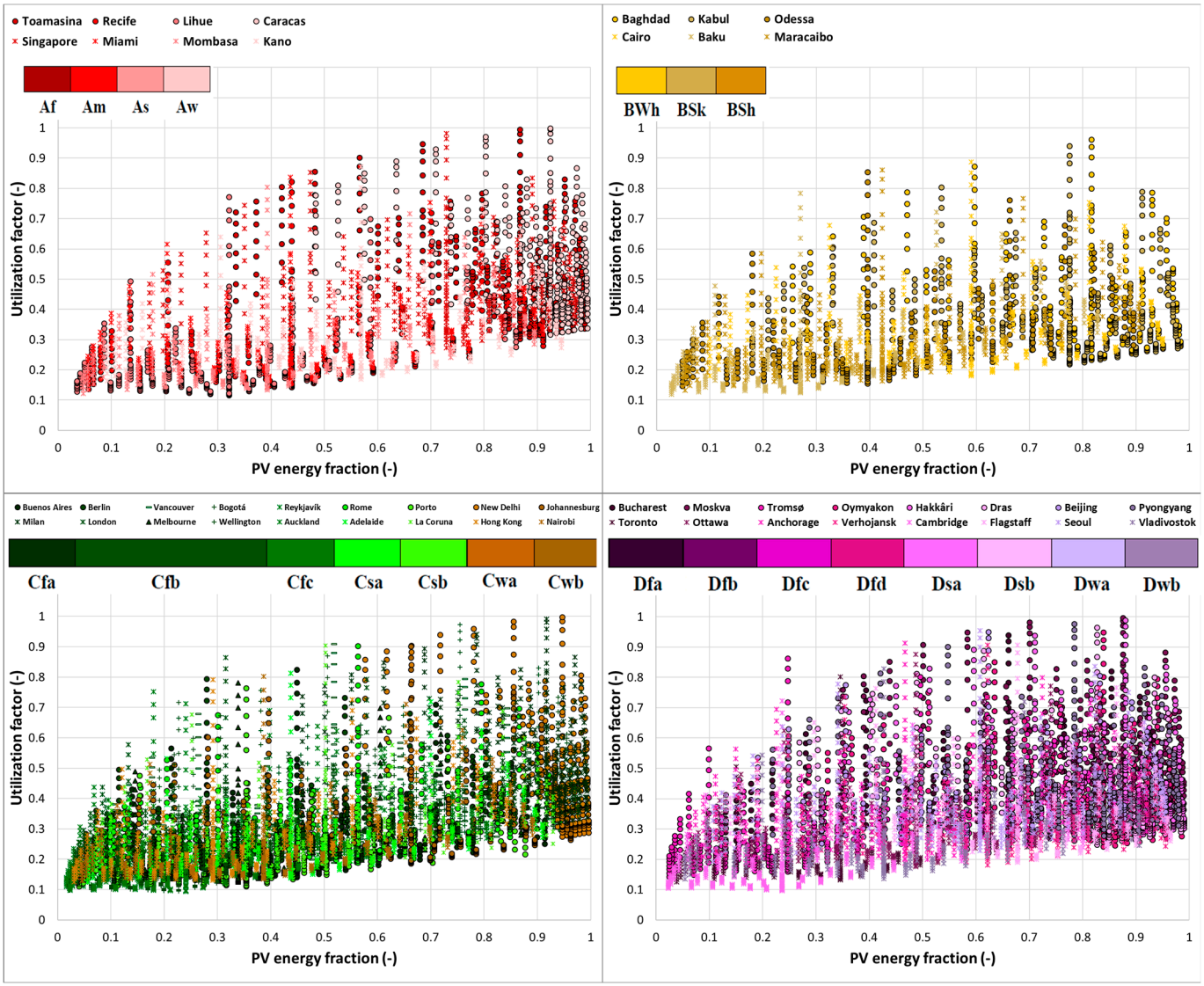

Figure 4. Utilization factor of 343 system power configurations across Köppen–Geiger climates.

As regards the GEIF of Figure 5, its range of variation decreases with increasing the PV energy fraction. A GEIF value of 0 indicates that there is zero interaction with the grid, indicating that meeting the load demand does not require any energy from the grid. Additionally, the energy transfer to the grid is zero, as any excess energy produced is fully managed by the battery system.

Quantitatively, the points of Group C and D vary in a wider range compared to Groups A and B with greater maximum values. In all climates, GEIF values of 0 are never reached, but they come very close. The highest GEIF value is about 10 and is reached in climate C, followed by climate zones D, A, and B. When the PV energy fraction is between 0.9 and 1, the GEIF is between 1 and 3. When the PV energy fraction is between 0 and 0.1, the GEIF is between 1 and 6 for climates A and B, and between 1 and 8 for climates C and D.

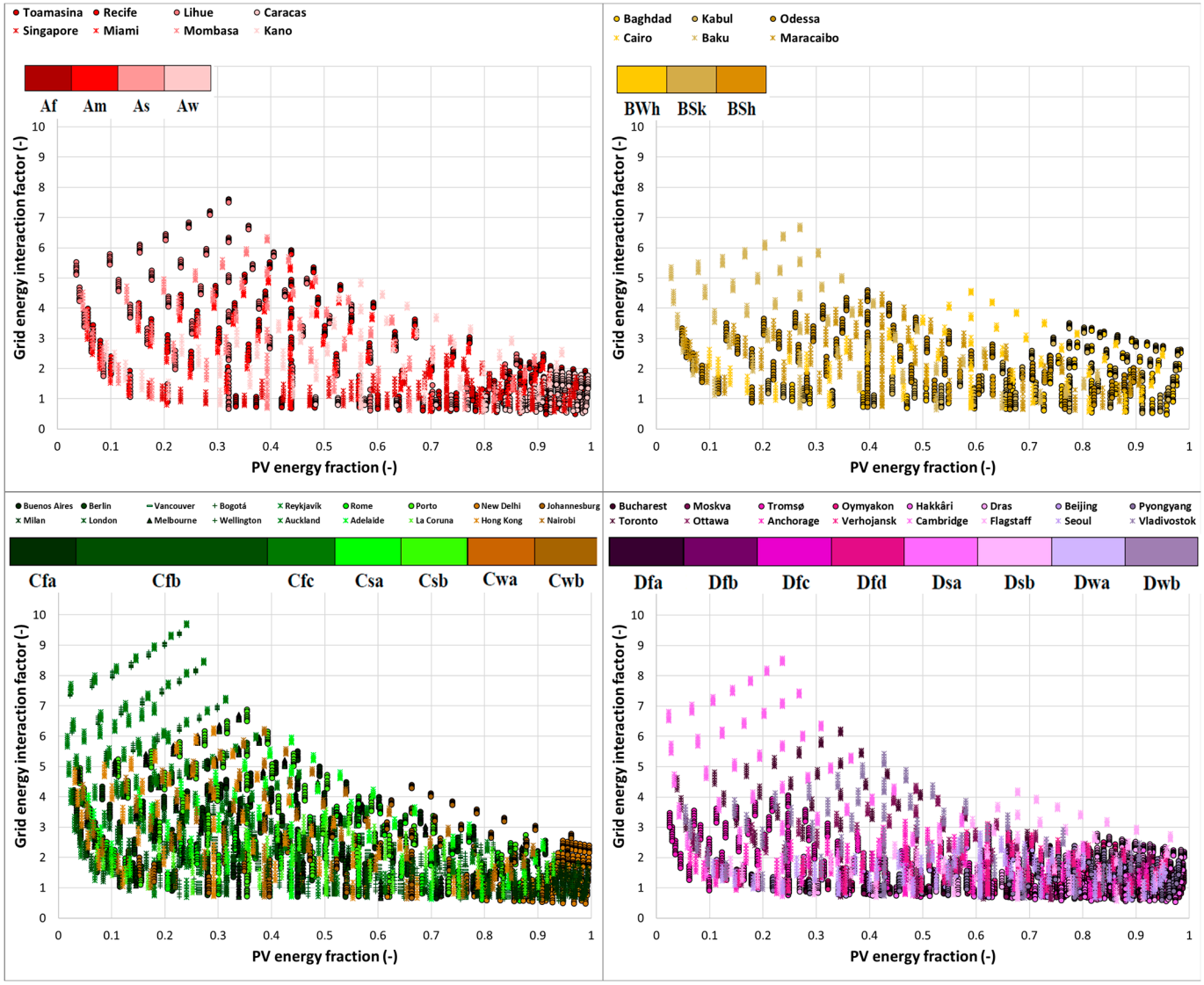

Figure 5. Grid energy interaction factor of 343 system power configurations across Köppen–Geiger climates.

Figures 6 and 7 illustrate the values obtained from the benefit-cost ratio (BCR) for SA and GC HRES, respectively, as a function of the PV energy fraction, represented by Köppen climate groups and sub-groups.

For SA HRES, no dependence of the BCR values on the PV energy fraction is highlighted. Only at the highest values of the PV energy fraction, a slight increase in BCR can be observed. Two localities belonging to As and Dsa appear to have very high values compared to the other localities. Except for these localities, Group C is characterized by a greater range of BCR variation until 0.05.

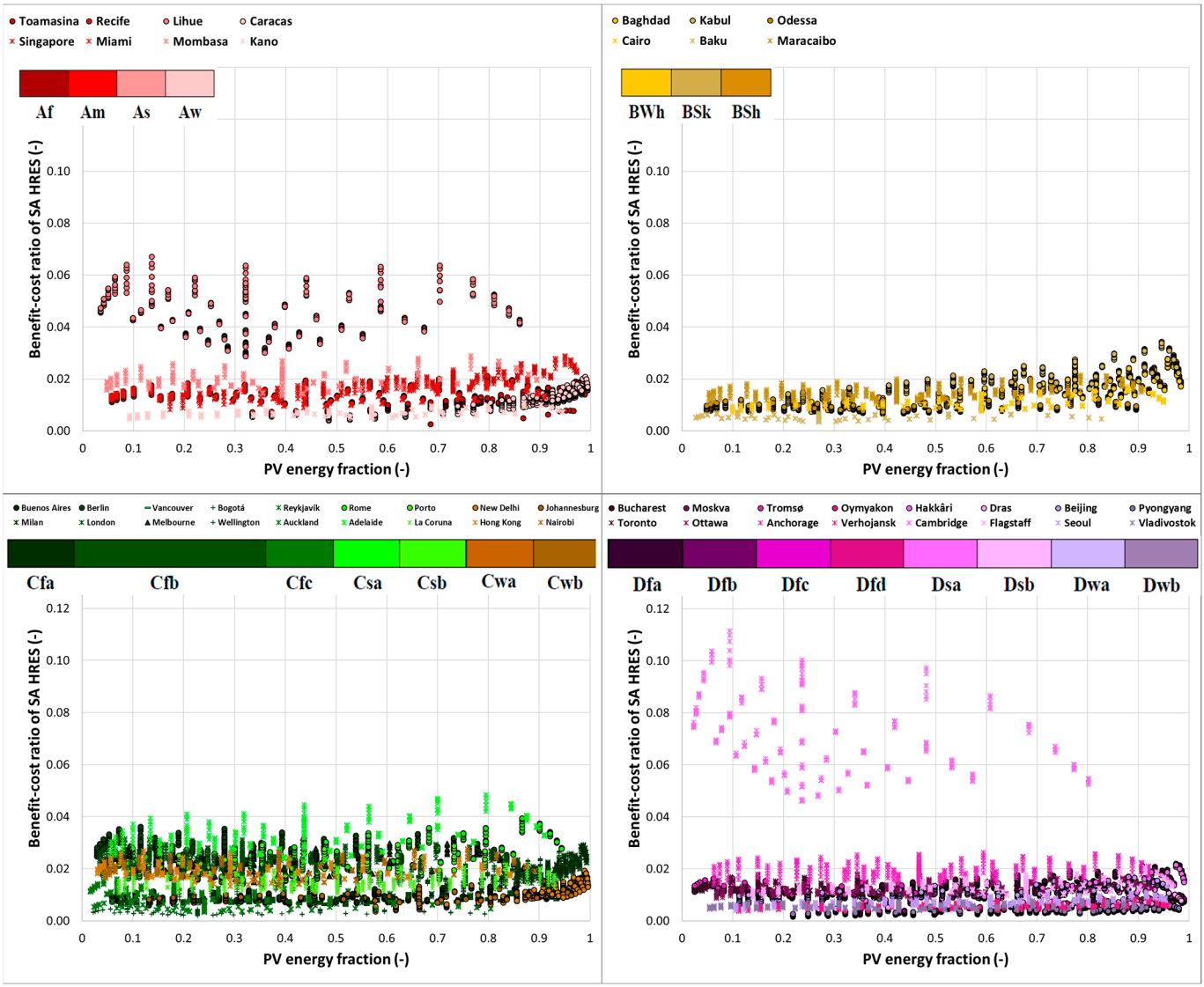

Figure 6. Benefit-cost ratio of 343 stand-alone (SA) system power configurations across Köppen–Geiger climates.

The BCR of GC HRES is significantly higher than SA HRES. The effect of FiT policies worldwide can be appreciated especially in Group A, where an increase in the PV energy fraction leads to a reduction in the BCR. The same trend can be observed for Group C, while Group D shows a trend with a minimum value around PV energy fraction values of 0.5. Contrarily to Group A, Group B is characterized by the lowest increase in BCR owing to the absence of economic FiT subsidy or the presence of underdeveloped countries. The independence of PV energy fraction is already highlighted for BCR, as previously revealed by the SA HRES.

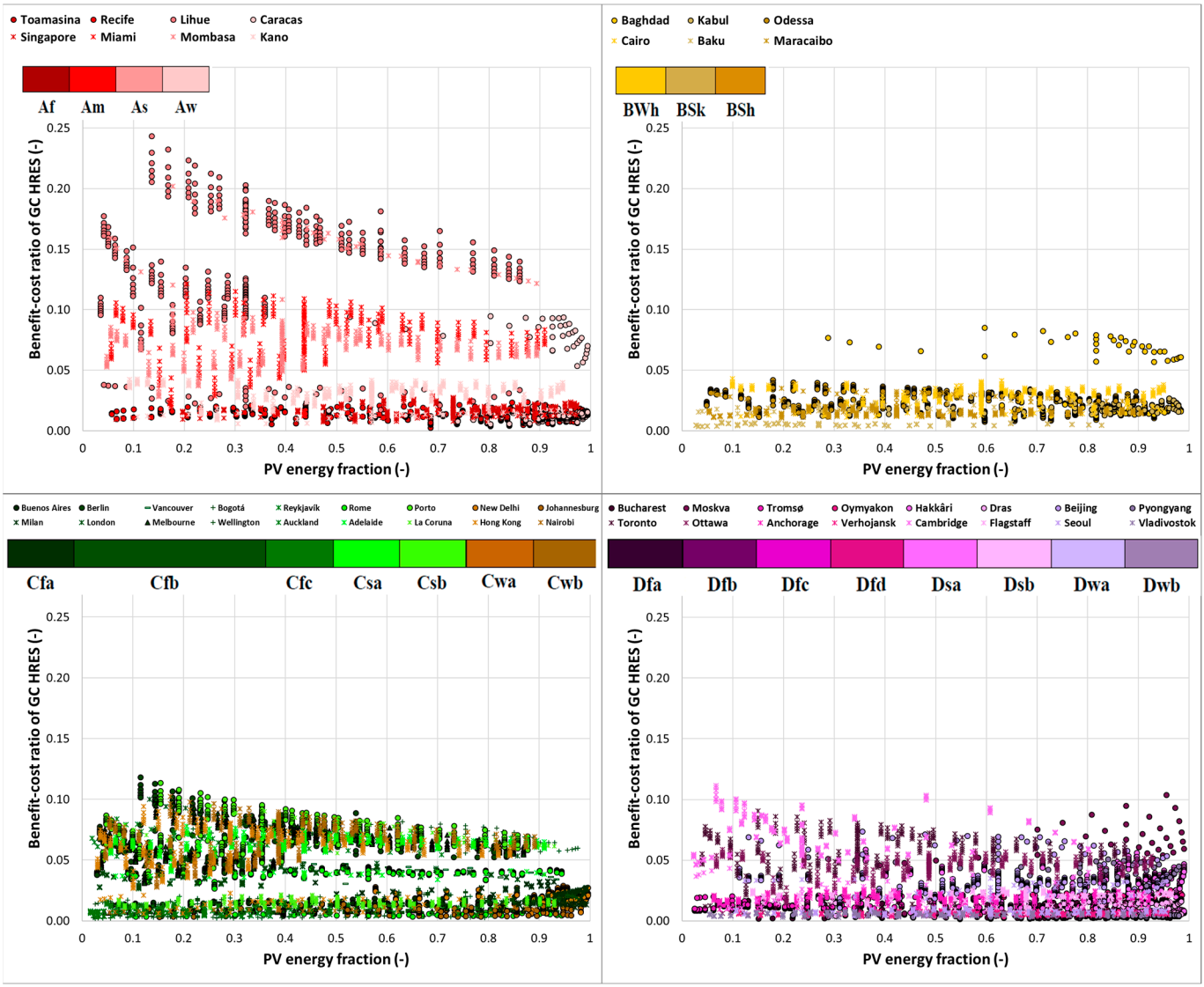

Figure 7. Benefit-cost ratio of 343 grid-connected (GC) system power configurations across Köppen–Geiger climates.

4. Conclusions

This study investigates the resilience of renewable PV–wind hybrid systems to different climate conditions. To this end, an extensive analysis of hybrid renewable systems behaviour is conducted to serve a small office community. It is necessary to operate electric lighting, electric office equipment, and charging stations for electric vehicles located in the parking lots of office buildings. Forty-eight locations are carefully selected across the Köppen climate classification to cover different latitudes, altitudes, and climatic conditions.

Using TRNSYS, the hourly power values of every component in the hybrid system were computed. These values were then employed to determine the annual energy contributions for the energy balances of both stand-alone and grid-connected systems. A parametric analysis was carried out for all of the chosen cities. The power outputs of the PV, wind, and battery systems ranged from 10 kW to 130 kW, with 20 kW increments, resulting in a total of 343 possible system power configurations.

This objective is pursued through hourly and annual dynamic analysis of the hybrid system and plant sustainability is assessed through technical and economic indicators.

The outcomes are summarized in the form of satisfied load fraction (SLF), utilization factor (UF), grid energy interaction factor (GEIF), and benefit-cost ratio (BCR). After ana-

lyzing the data, it was determined that it is difficult to achieve a high satisfied load fraction with a low proportion of PV.

The highest SLF values are obtained with a significant prevalence of PV over wind power, the trend being more pronounced for climate zones B and D. Climate A and climate C achieve an SLF value of 1 already from a PV energy fraction of 0.2, while climates B and D from a PV energy fraction of 0.5.

Solar or wind energy alone cannot fully meet the load at all locations. Group B shows lower utilization factors than the other groups, denoting high energy excess. For groups A, C, and D, a strong concentration is evident for high values of PV energy fraction and tendentially lower values of utilization fraction. Values of UF equal to 1 are rarely reached and never by extreme values of PV energy fraction (and thus considering only wind or only PV contributions).

In all climates, it is evident that the GEIF values of zero are never reached, but they come very close.

For stand-alone, no dependence of BCR on PV energy fraction is shown. Only for high values of the PV fraction is a slight increase in BCR observed.

The benefit-cost ratio (BCR) is higher for grid-connected systems than stand-alone ones. The impact of FiT policies around the world is particularly evident in tropical climates (Group A), where increasing the PV energy fraction results in a decrease in BCR. This trend is also observed in temperate climates (Group C), while continental climates (Group D) exhibit a trend with a minimum value around PV fraction values of 0.5.

Author Contributions: Conceptualization, N.M., D.M., C.B. and P.M.C.; methodology, N.M., D.M., C.B. and P.M.C.; software, N.M., D.M., C.B. and P.M.C.; validation, N.M., D.M., C.B. and P.M.C.; formal analysis, N.M., D.M., C.B. and P.M.C.; investigation, N.M., D.M., C.B. and P.M.C.; data curation, N.M., D.M., C.B. and P.M.C.; writing—original draft preparation, N.M., D.M., C.B. and P.M.C.; writing—review and editing, N.M., D.M., C.B. and P.M.C.; visualization, N.M., D.M., C.B. and P.M.C.; supervision, N.M., D.M., C.B. and P.M.C. All authors have read and agreed to the published version of the manuscript.

Funding: This research received no external funding.

Data Availability Statement: Data will be made available on request.

Conflicts of Interest: The authors declare no conflict of interest.

Nomenclature

B	Yearly benefit	€/yr
C	Overall system cost	€
BCR	Benefit-cost ratio	
E_g	Yearly energy produced by the generators	Wh
E_l	Yearly energy required by the load	Wh
$e_{pv,g}$	PV energy fraction	
E_{tl}	Yearly produced energy sent to the load	Wh
FiT	Feed-in-Tariff	
GC	Grid-connected	
GEIF	Grid energy interaction factor	
HRES	Hybrid renewable energy system	
IEA	International Energy Agency	
NOCT	Nominal operating temperature	°C
PV	Photovoltaic	
SA	Stand-alone	
SLF	Satisfied load fraction	
UF	Utilization factor	

References

1. Congedo, P.M.; Baglivo, C. Implementation hypothesis of the Apulia ITACA Protocol at district level—Part I: The model. *Sustain. Cities Soc.* **2021**, *70*, 102931. [CrossRef]
2. Congedo, P.M.; Baglivo, C.; Toscano, A.M. Implementation hypothesis of the Apulia ITACA Protocol at district level—Part II: The case study. *Cities Soc.* **2021**, *70*, 102927. [CrossRef]
3. Bueno, S.; Bañuls, V.A.; Gallego, M.D. Is urban resilience a phenomenon on the rise? A systematic literature review for the years 2019 and 2020 using textometry. *Int. J. Disaster Risk Reduct.* **2021**, *66*, 102588. [CrossRef]
4. Büyüközkan, G.; Ilıcak, Ö.; Feyzioğlu, O. A review of urban resilience literature. *Sustain. Cities Soc.* **2022**, *77*, 103579. [CrossRef]
5. Baglivo, C.; Congedo, P.M.; Mazzeo, D. 3-Scenarios for urban resilience—Perspective on climate change resilience at the end of the 21st century of a photovoltaic-powered mixed-use energy community in two European capitals. In *Woodhead Publishing Series in Civil and Structural Engineering, Adapting the Built Environment for Climate Change*; Fernando Pacheco-Torgal, F., Granqvist, C.G., Eds.; Woodhead Publishing: Sawston, UK, 2023; pp. 37–52. ISBN 9780323953368. [CrossRef]
6. O'Farrell, P.; Anderson, P.; Culwick, C.; Currie, P.; Kavonic, J.; McClure, A.; Ngenda, G.; Sinnott, E.; Sitas, N.; Washbourne, C.-L.; et al. Towards resilient African cities: Shared challenges and opportunities towards the retention and maintenance of ecological infrastructure. *Glob. Sustain.* **2019**, *2*, e19. [CrossRef]
7. Sajjad, M.; Chan, J.C.L.; Chopra, S.S. Chopra, Rethinking disaster resilience in high-density cities: Towards an urban resilience knowledge system. *Sustain. Cities Soc.* **2021**, *69*, 102850. [CrossRef]
8. Mou, Y.; Luo, Y.; Su, Z.; Wang, J.; Liu, T. Evaluating the dynamic sustainability and resilience of a hybrid urban system: Case of Chengdu, China. *J. Clean. Prod.* **2021**, *291*, 125719. [CrossRef]
9. Galvan, E.; Mandal, P.; Sang, Y. Networked microgrids with roof-top solar PV and battery energy storage to improve distribution grids resilience to natural disasters. *Int. J. Electr. Power Energy Syst.* **2020**, *123*, 106239. [CrossRef]
10. Jamaluddin, K.; Alwi, S.R.W.; Manan, Z.A.; Hamzah, K.; Klemeš, J.J. Hybrid power systems design considering safety and resilience. *Process Saf. Environ. Prot.* **2018**, *120*, 256–267. [CrossRef]
11. Stirling, A. From sustainability, through diversity to transformation: Towards more reflexive governance of technological vulnerability. In *Vulnerability in Technological Cultures: New Directions in Research and Governance*; Hommels, A., Mesman, J., Bijker, W.E., Eds.; Inside Technology; MIT Press: Cambridge, MA, USA, 2014.
12. Kosai, S.; Unesaki, H. Short-term vs long-term reliance: Development of a novel approach for diversity of fuels for electricity in energy security. *Appl. Energy* **2020**, *262*, 114520. [CrossRef]
13. Winzer, C. Conceptualizing energy security. *Energy Policy* **2012**, *46*, 36–48. [CrossRef]
14. Menyah, K.; Wolde-Rufael, Y. CO_2 emissions, nuclear energy, renewable energy and economic growth in the US. *Energy Policy* **2010**, *38*, 2911–2915. [CrossRef]
15. Mazzeo, D.; Matera, N.; De Luca, P.; Baglivo, C.; Congedo, P.M.; Oliveti, G. A literature review and statistical analysis of photovoltaic-wind hybrid renewable system research by considering the most relevant 550 articles: An upgradable matrix literature database. *J. Clean. Prod.* **2021**, *295*, 126070. [CrossRef]
16. Baglivo, C. Dynamic Evaluation of the Effects of Climate Change on the Energy Renovation of a School in a Mediterranean Climate. *Sustainability* **2021**, *13*, 6375. [CrossRef]
17. Ellabban, O.; Abu-Rub, H.; Blaabjerg, F. Renewable energy resources: Current status, future prospects and their enabling technology. *Renew. Sustain. Energy Rev.* **2014**, *39*, 748–764. [CrossRef]
18. Sapkota, A.; Lu, Z.; Yang, H.; Wang, J. Role of renewable energy technologies in rural communities' adaptation to climate change in Nepal. *Renew. Energy* **2014**, *68*, 793–800. [CrossRef]
19. Matera, N.; Mazzeo, D.; Baglivo, C.; Congedo, P.M. Hourly forecasting of the photovoltaic electricity at any latitude using a network of artificial neural networks. *Sustain. Energy Technol. Assess.* **2023**, *57*, 103197. [CrossRef]
20. Mazzeo, D.; Baglivo, C.; Matera, N.; Congedo, P.M.; Oliveti, G. A novel energy-economic-environmental multi-criteria decision-making in the optimization of a hybrid renewable system. *Sustain. Cities Soc.* **2020**, *52*, 101780. [CrossRef]
21. Baglivo, C.; Mazzeo, D.; Oliveti, G.; Congedo, P.M. Technical data of a grid-connected photovoltaic/wind hybrid system with and without storage battery for residential buildings located in a warm area. *Data Brief* **2018**, *20*, 587–590. [CrossRef]
22. Hurtado, E.; Peñalvo-López, E.; Pérez-Navarro, Á.; Vargas, C.; Alfonso, D. Optimization of a hybrid renewable system for high feasibility application in non-connected zones. *Appl. Energy* **2015**, *155*, 308–314. [CrossRef]
23. Ogunjuyigbe, A.S.O.; Ayodele, T.R.; Akinola, O.A. Optimal allocation and sizing of PV/Wind/Split-diesel/Battery hybrid energy system for minimizing life cycle cost, carbon emission and dump energy of remote residential building. *Appl. Energy* **2016**, *171*, 153–171. [CrossRef]
24. World Bank. Access to electricity (% of population). Dataworldbankorg. 2010.
25. IEA. *Data and Statistics*; International Energy Agency—IEA: Paris, France, 2014.
26. Sanajaoba, S. Optimal sizing of off-grid hybrid energy system based on minimum cost of energy and reliability criteria using firefly algorithm. *Sol. Energy* **2019**, *188*, 655–666. [CrossRef]
27. Ma, J.; Yuan, X. Techno-economic optimization of hybrid solar system with energy storage for increasing the energy independence in green buildings. *J. Energy Storage* **2023**, *61*, 106642. [CrossRef]
28. Khan, F.A.; Pal, N.; Saeed, S.H.; Yadav, A. Modelling and techno-economic analysis of standalone SPV/Wind hybrid renewable energy system with lead-acid battery technology for rural applications. *J. Energy Storage* **2022**, *55 Pt D*, 105742. [CrossRef]

29. El-Sattar, H.A.; Sultan, H.M.; Kamel, S.; Khurshaid, T.; Rahmann, C. Optimal design of stand-alone hybrid PV/wind/biomass/battery energy storage system in Abu-Monqar, Egypt. *J. Energy Storage* **2021**, *44 Pt A*, 103336. [CrossRef]
30. Kosai, S.; Cravioto, J. Resilience of standalone hybrid renewable energy systems: The role of storage capacity. *Energy* **2020**, *196*, 117133. [CrossRef]
31. Congedo, P.M.; Baglivo, C.; Seyhan, A.K. Raffaele Marchetti, Worldwide dynamic predictive analysis of building performance under long-term climate change conditions. *J. Build. Eng.* **2021**, *42*, 103057. [CrossRef]
32. Congedo, P.M.; Baglivo, C.; D'Agostino, D.; Mazzeo, D. The impact of climate change on air source heat pumps. *Energy Convers. Manag.* **2023**, *276*, 116554. [CrossRef]
33. Mazzeo, D. Nocturnal electric vehicle charging interacting with a residential photovoltaic-battery system: A 3E (energy, economic and environmental) analysis. *Energy* **2019**, *168*, 310–331. [CrossRef]
34. Mazzeo, D.; Matera, N.; De Luca, P.; Baglivo, C.; Congedo, P.M.; Oliveti, G. Worldwide geographical mapping and optimization of stand-alone and grid-connected hybrid renewable system techno-economic performance across Köppen-Geiger climates. *Appl. Energy* **2020**, *276*, 115507. [CrossRef]
35. Mitsubishi Electric & Electronics USA, Inc. Mitsubishi PV-MLU250HC. Available online: https://www.mitsubishielectricsolar.com/images/uploads/documents/specs/MLU_spec_sheet_250W_255W.pdf (accessed on 15 November 2022).
36. Renugen—Renewable Generation, Tulipower 2.5kW Wind Turbine. Available online: https://www.renugen.co.uk/tulipower-2-5kw-wind-turbine-discontinued (accessed on 23 June 2020).
37. Electric Car Home, sonnenBatterie. Available online: https://electriccarhome.co.uk/battery-storage/sonnen-battery (accessed on 15 November 2022).
38. Solaris Technology Industry, Inc., Fronius. Available online: https://www.solaris-shop.com/fronius-ig-plus-v-5-0-1-uni-5-0kw-inverter-4-210-113-800 (accessed on 15 November 2022).
39. University of Wisconsin. Solar Energy Laboratory, TRNSYS 17: A Transient System Simulation Program. 2012. Available online: http://www.trnsys.com/ (accessed on 26 April 2020).
40. Fry, B.A. Simulation of Grid-Tied Building Integrated Photovoltaic Systems. Master's Thesis, Solar Energy Laboratory, University of Wisconsin, Madison, WI, USA, 1999.
41. Quinlan, P.J.A. Time Series Modeling of Hybrid Wind Photovoltaic Diesel Power Systems. Master's Thesis, Solar Energy Laboratory, University of Wisconsin, Madison, WI, USA, 1996.
42. Mazzeo, D.; Oliveti, G.; Baglivo, C.; Congedo, P.M. Energy reliability-constrained method for the multi-objective optimization of a photovoltaic-wind hybrid system with battery storage. *Energy* **2018**, *156*, 688–708. [CrossRef]